Journal of Automation and Intelligence 2 (2023) 31–41

Contents lists available at ScienceDirect

Journal of Automation and Intelligence

journal homepage: www.keaipublishing.com/en/journals/journal-of-automation-and-intelligence/

Towards cognitive navigation: A biologically inspired calibration mechanism for the head direction cell network

Zhenshan Bing [a,*], Dominik Nitschke [a], Genghang Zhuang [a], Kai Huang [b], Alois Knoll [a]

[a] Department of Informatics, Technical University of Munich, Munich, 85741, Germany
[b] School of Data and Computer Science, Sun Yat-sen University, Guangzhou, 510006, China

ARTICLE INFO

Keywords:
Head direction cells
Error calibration
Cognitive navigation
Neural SLAM

ABSTRACT

To derive meaningful navigation strategies, animals have to estimate their directional headings in the environment. Accordingly, this function is achieved by the head direction cells that were found in mammalian brains, whose neural activities encode one's heading direction. It is believed that such head direction information is generated by integrating self-motion cues, which also introduces accumulative errors in the long term. To eliminate such errors, this paper presents an efficient calibration model that mimics the animals' behavior by exploiting visual cues in a biologically plausible way, and then implements it in robotic navigation tasks. The proposed calibration model allows the agent to associate its head direction and the perceived egocentric direction of a visual cue with its position and orientation, and therefore to calibrate the head direction when the same cue is viewed again. We examine the proposed head direction calibration model in extensive simulations and real-world experiments and demonstrate its excellent performance in terms of quick association of information to proximal or distal cues as well as accuracy of calibrating the integration errors of the head direction. Videos can be viewed at https://videoviewsite.wixsite.com/hdc-calibration.

1. Introduction

To survive in the wild, animals have to navigate efficiently through their environment, even under constantly changing conditions, like the time of the year or the weather. The brilliant navigation skills of animals are brought about by the cognitive map in their brains, which is formed by the neural representations of spatial information about the environment [1]. This cognitive map allows many animals, like sea turtles, wolves, bears, and homing pigeons, to return to their home bases even over hundreds of kilometers and long periods of time [2–6]. The mechanism of creating a cognitive map by integrating spatial information, while using it to navigate, is believed to be relevant to several types of spatially modulated cells, such as head direction cells (HDCs) [7], grid cells (GCs) [8], and place cells (PCs) [9].

One central part for the derivation of meaningful navigation strategies is the estimation of one's head direction [10]. The so-called head direction cells (HDCs), discovered in many species [11–15], were reported to undertake this function by firing corresponding to one's head direction (HD) with respect to the environment, but independent of the animal's location or the ambient conditions of the environment. Therefore, HDCs are believed to state the sense of spatial orientation of animals by integrating self-motion cues from the vestibular system, like the animal's angular velocity [14]. The process of integrating such self-motion information is often referred to as path integration, which allows, for example, rats to estimate their orientation even in darkness [16]. However, accumulative errors will be inevitably introduced to the HD signal during the process of path integration [17].

Inspired by the fact that animals utilize landmark information (from e.g. olfactory or visual cues) to correct HD errors [14], this work aims to address the problem of how the HD signal can be calibrated using the directional information derived from egocentrically perceived landmarks. State-of-the-art HDC calibration models can be generally divided into two categories. Models in the first category directly infer the HD signal from the egocentric cue direction (ECD), which describes the perceived angular direction of a visual landmark in the egocentric frame [18,19]. These models are only applicable to environments in which the positional relationship between the agent and the cue is constant, for example, when the visual cue is in infinite distance. In this case, the cue acts like a compass and is used to infer one's head direction. The second category contains calibration models that associate a combination of ECD information and the position of the agent with the HD signal [20–22]. Subsequently, these models can infer the HD information from perceiving a visual landmark from a known position and orientation in the environment. Therefore, unlike the models in the first category, these models can cope with proximal landmarks as well. However, these methods are inefficient due to the fact that they can only calibrate the HD signal when perceiving a

* Corresponding author.
E-mail address: zhenshan.bing@tum.de (Z. Bing).

https://doi.org/10.1016/j.jai.2023.100020
Received 19 December 2022; Received in revised form 24 January 2023; Accepted 31 January 2023

landmark a second time on the exact same location with the same orientation.

To this end, this paper presents a new biologically plausible computational model that efficiently facilitates the correction of HD errors arising from path integration using a visual landmark. In contrast to existing simple place encoding models [20,21], the proposed model is able to calibrate the HD signal when the visual cue is perceived again, regardless of the agent's position or orientation, which leads to much more efficient calibration. The proposed calibration model is proven to be accurate and applicable to be used in real-world robotic tasks. The contributions of this work are summarized as follows.

- We propose a novel HDC calibration model that efficiently uses the egocentrically perceived angular direction of a visual cue in combination with positional information of an exploring agent to correct for HD errors introduced by path integration. This proposed model allows an agent to calibrate its HD signal from any locations where the visual cue can be perceived again.
- As one part of the calibration model, we propose a neural circuit based on two two-dimensional conjunctive cells, which allows the model to continuously compute the global direction of a visual cue from a certain location (allocentric cue direction, ACD), given the ECD and HD information during exploration. In turn, the restored ACD can be used to compute the HD with perceived ECD for calibration.
- As one part of the calibration model, we propose a novel place encoding strategy for calibrating the HD signal, which is named as first glance learning (FGL). Compared with the simple place field encoding strategy [20,21], FGL allows the agent to calibrate the HD signal independent of its position or orientation, leading to more calibration opportunities.
- We demonstrate the accuracy of the HD error calibration model by testing it in both simulated environments and real-world scenarios. Experimental results show that the model is able to effectively and efficiently calibrate the HD signal with a distal or proximal visual landmark.

2. Biology background

In this section, we first briefly describe the experimental findings about information sources and reference frames that are used by animals for the spatial navigation task. Secondly, we present a selection of spatially modulated cells that are found in the brain and are thought to serve as a mental representation of the environment.

2.1. Navigation cues

Rodents can integrate multi-modal sensory information to construct an internal representation of the environment [23]. The sources of information can be categorized into two kinds, namely, the allothetic and idiothetic ones [23,24]. Allothetic information lies externally to the body of the animal [25], which are features or properties of the environment [23]. An animal can derive allothetic information from environmental properties by using different sensory modalities, including the visual, auditory, and olfactory system [25]. By contrast, idiothetic information is self-referential and also referred to as internal cues [24]. It allows the animal to calculate its position as well as allothetic cues, but without the need for prior knowledge about the environment as only self-information is integrated. Idiothetic information can be generated from the vestibular system, the proprioception, and the motor system [26,27]. It was found that, for example, the brain improves the estimation of position and orientation by using a combination of different sensory information [28].

2.2. Navigation references

Animals make use of a variety of stimulus sources that correspond to mainly two frames of Ref. [29], namely, the allocentric and the egocentric reference frame. The allocentric reference frame's coordinates are external to the animal and world-centered [23]. It is anchored in to a fixed location of the environment [30,31]. For example, the HD signal of an animal within the environment is a spatial information that is processed in the allocentric frame. The egocentric reference's coordinates are defined relative to the animal itself, and therefore is body-centered [31]. The coordinates are anchored to the animal's pose and change along with the rotation and translation of the animal [23]. For instance, the perception of a visual cue is facilitated in the egocentric frame. Therefore, the egocentric perception of the angular direction of the cue depends on the animal's position and orientation [30,31].

2.3. Spatially modulated cells

The firing property of spatially modulated cells represents environmental features and can serve as a mental representation of the environment [23,32,33]. In the following, cells that are thought to be important for navigation and used in this paper are briefly described. All cells are either proven to exist biologically, for example, in rat brains, or at least proposed by other researchers.

2.3.1. Head direction cells

HDCs fire according to the animal's head direction, or rather its allocentric orientation, in reference to the external environment regardless of the animal's position [11,16,28,34,35]. Therefore, HDCs function as an internal neural compass, and consequently serve as the fundamental base for spatial navigation [23]. Transformations between egocentric coordinates (of e.g. sensory feature angles) and allocentric coordinates (location of environmental features) can be facilitated with the help of the HD signal [36,37].

2.3.2. Egocentric cue direction cells

ECD cells encode the direction of a cue in the egocentric coordinates [38]. Evidence for cells that resemble view-dependent direction encoding of visual cues were found in [38,39]. For example, if an animal is positioned in an environment with one visual cue, the ECD cells will encode the direction in which the visual landmark lies with reference to the animal's orientation (See Fig. 1). Computational models of ECD cells can be found in [18,19]. More formal definition of ECD cells can be found in Section 4.4.2.

2.3.3. Allocentric cue direction cells

ACD cells are supposed to fire in relation to the direction of a cue in the allocentric coordinates [30]. In this case, the direction encoded by these cells is solely dependent on the animal's current position and independent from its orientation. ACD cells have not been reported yet, but are predicted by a computational model from [40]. Their firing behavior could be generated by combining information from ECD cells and HDCs [40] and one example is shown in Fig. 1.

2.3.4. Conjunctive cells

Conjunctive cells were discovered by [38]. These neurons are thought to be aligned in a grid, and therefore form a two-dimensional conjunctive cell field that combines the encoding of allocentric and egocentric reference frames via a two-dimensional activity peak, where one dimension encodes the HD (allocentric) and the other dimension encodes the ECD (egocentric) of a visual cue [38].

2.3.5. Place cells

Place cells were discovered in the hippocampus of rats for the first time by [41]. This population of cells is sensitive to an animal's location within the environment [41]. When an animal enters a certain place field, the corresponding place cell's firing activity increases.

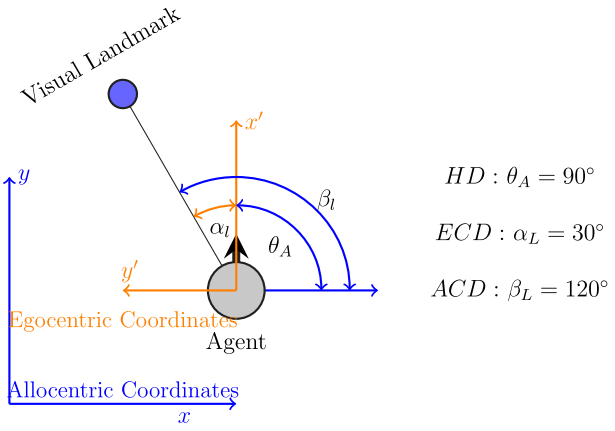

Fig. 1. The spatial relation between an agent and a visual landmark.

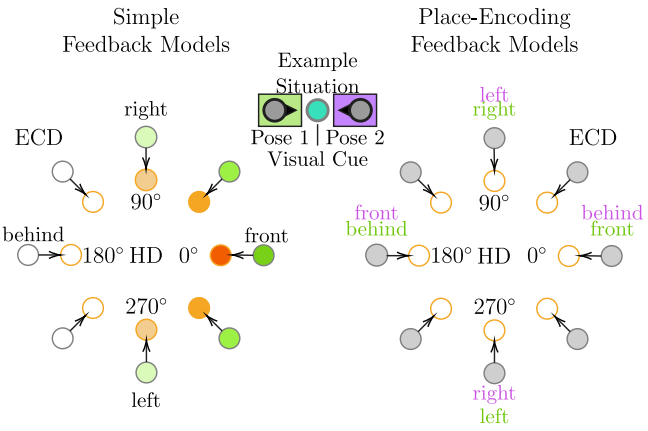

Fig. 2. The two main types of HD calibration models. Left: simple feedback models consist of two rings of neurons. The outer ring encodes the ECD of a perceived visual landmark and directly projects onto the inner ring which encodes HD. Right: place-encoding feedback models associate the information about the agent's position with the current perceived ECD to infer HD. Their setup can be imagined as using several ECD rings that directly drive the HD.

3. Related work

Existing HD calibration models can be divided into two categories according to the usage of allothetic information. The first category contains simple feedback models that use the egocentric cue information as the single source of allothetic information to infer the HD information. The second category, the place encoding models, use a combination of ECD and positional information of an agent to infer its HD.

3.1. Simple feedback models

Simple feedback models use the perceived ECD of a visual cue as a single source of allothetic information to directly infer the HD signal. The general setup is shown in the left part of Fig. 2. Simple feedback models consist mainly of two rings of neurons. The outer ring consists of ECD cells which directly project onto the inner ring that is composed of HDCs. Taking "Pose 1" as an example, the agent perceives the visual cue in its front direction. Therefore, the ECD cell representing "front" is the most active neuron and drives the HD cell to represent 0°, which is in accordance with the agent's orientation. If the spatial relation between an agent and a visual cue in the environment is stable, these models can sufficiently derive the HD information from the egocentric perception of a visual cue. It must be noted that this model only works properly under two conditions. Either the visual cue is in infinite distance, or the agent's freedom of movement is limited to a straight line originating from the landmark's position. This ensures that the ECD always has the same offset to the HD.

Zhang [18] proposed a simple feedback model that uses a continuous attractor neural network consisting of two rings to encode the current estimation of HD by integrating angular velocity input from the agent. A third outer ring, composed of ECD cells, encodes the ECD of a visual landmark. The ECD cells directly project onto one of the two rings of HDCs via one-to-one connections. The connection weights are learned via one-shot Hebbian learning at the first view of the landmark. Subsequently, the ECD cells control the neural activities in both HD rings to correct for accumulative HD errors. Another simple feedback model from [19] used a similar approach to calibrate the HD signal. However, the visual feature detectors have constantly Hebbian-learning connections to all HDCs, which allows the model to connect the HD representation to spatially stable landmarks and to disconnect from unstable landmarks.

3.2. Place-encoding feedback models

The second category, the place encoding feedback models, uses the perceived ECD of a visual cue to infer HD according to the current position of the agent around the landmark. The right part of Fig. 2 illustrates the general concept of place-encoding feedback models. The inner ring consists of HDCs. The outer ring consists of ECD cells that encode the ECD of the visual landmark depending on the agent's current position. The ECD cells project again directly onto the HDCs. Taking "Pose 1" as an example, when the agent is located in the green field, the ECD cells will correspond to the ECDs labeled in green, which is identical to the setup of the simple feedback model. However, for "Pose 2", the right neuron in the ECD ring represents the ECD "front" when the agent is in the purple field of the example situation and corresponds to 180° in the HD layer. In this case, the ECD cells according to the green labels would introduce a huge HD error. Therefore, the second set of ECD cells corresponding to the purple labels is active and indicates the correct HD of the agent when located in the purple field. By doing this, place-encoding feedback models can derive HD information from proximal cues as well as from distal cues.

The place-encoding feedback model from [20] used neuron sheets that act as position dependent interface to associate HD with ECD. The model encodes the ECD of a visual landmark via a visual sensory input, similar to ECD cells. The place-encoding feedback model from [21] used only one set of interface neurons, called calibration cells, to infer HD from ECD and positional information about the agent. Each calibration cell receives input via learning connections from both the visual sensory input that encodes the ECD of a visual landmark and the position encoding cells. Milford et al. [22] proposed a place-encoding feedback model that uses two three-dimensional attractor cell networks. A pose cell network encodes the position of the agent in two dimensions and the orientation of the agent in the third dimension, such that a three-dimensional activity packet describes an agent's pose completely. Some other works also use visual information to calibrate integration error [42].

4. Modeling of neural circuit

This section presents the computation model of the proposed HDC calibration mechanism. We first provide an overview of the calibration system and then the computation model of each component. Finally, we explain the general procedure to compute the synaptic connections between different components within the system.

4.1. Overview

The architecture of the proposed HD calibration system is shown in Fig. 3. It consists of two major neural circuits, namely, the basic

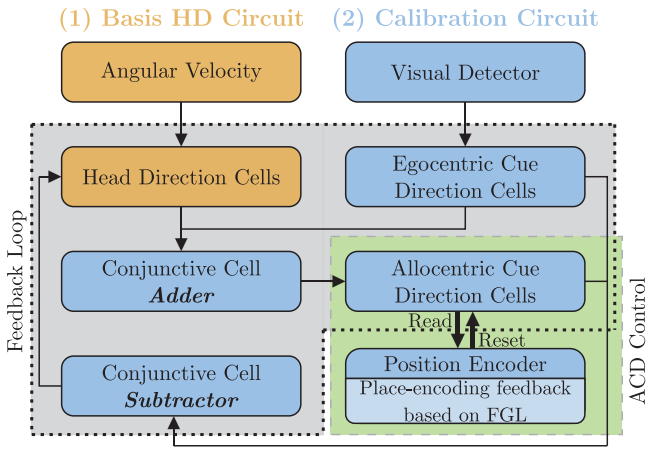

Fig. 3. Architecture of the proposed HD calibration model: (1) The basis HD circuit indicates the current estimation of HD by integrating the angular velocity input via the HDCs. (2) The calibration circuit facilitates learning and exploiting of directional information from visual landmarks. When the visual detector input is active, ACD information is created by combining HD with ECD information via the *Adder*. The position encoder either stores the ACD from the ACD cells or resets the activity of the ACD cells corresponding to the current position of the agent. The feedback signal back onto the HDCs is generated by combining ACD with ECD information via the *Subtractor*.

HDC circuit and its calibration circuit. The HDC circuit is reused from our previous work [43], which mimics the path integration process by integrating the angular velocity of an agent and estimating its head direction. The principle of the calibration circuit is to reset the head direction with the help of a fixed visual landmark in three steps.

- When the landmark is perceived for the first time, the egocentric direction of the visual cue can be obtained by the egocentric cue direction cells. Then, the allocentric direction of the cue can be calculated via the *Adder* with the information of the head direction and the egocentric direction of the cue.
- The allocentric direction of the cue is stored in the allocentric cue direction cells and this information is associated with the position of the agent by the position encoder.
- When the landmark is in sight again at any other position, the allocentric direction of the visual cue will be reset. Then, the ACD cells and ECD cells project together onto the *Subtractor*, which in turn calibrates the corresponding head direction of the agent.

4.2. Neuron model

The neural activity of a biological neuron is described with its firing rate, which is determined by the synaptic input from other neurons. In this paper, the activity of a neuron model supported by in vivo data [44] is used and modeled as

$$\tau \frac{df_i}{dt} = -f_i + \Phi(I_i + \sum_j w_{ij} f_j) = -f_i + \Phi(u_i). \tag{1}$$

f_i is the firing rate of neuron i. τ is a time constant. I_i is the external inputs to neuron i. w_{ij} is the connection (synaptic) weight from neuron j to neuron i. u_i is the total synaptic input to neuron i. $\Phi(\cdot)$ is the single-neuron transfer function, which is defined in our prior work [43]. According to (1), the firing rate of a neuron will always converge to the sigmoid term

$$f_i = \Phi(I_i + \sum_j w_{ij} f_j) = \Phi(u_i). \tag{2}$$

4.3. Head direction cell network

The HDC network is designed to estimate the directional heading of the system only relying on its angular velocity. As mentioned above, this work is built on the basis of the HDC network proposed in our previous work [43]. To ensure a general understanding of the HDC network, we briefly describe its architecture and functionality. More detailed information can be found in [43].

The HDC network consists of three ring layers of neurons, namely, the HDC layer and two shift layers to shift the peak activity of the HDC layer to the left or right direction. Additionally, two turning cells are used to inject turning stimuli to the HDC network, whose activities are calculated based on the angular velocity. The HDC layer represents the directional heading of the system and consists of n head direction cells. Their preferred direction θ_i ($i \in [0, \dots, n-1]$) is equally distributed around the circle and given in radians in the interval $[0, 2\pi)$. Each cell in the shift layer is associated with one cell in the HDC layer. Take one shift left cell as an example, it is connected to the HDCs on the left side of its corresponding HDC with excitatory synapses and to the other half with inhibitory synapses. When the agent turns left, the turning left cell will inject stimuli to all the cells in the shift left layer and therefore shift the activity of the HDC layer, which represents the head direction.

4.4. Calibration circuit

There are six components in the calibration circuit, namely, the visual detector, egocentric cue direction (ECD) cells, allocentric cue direction (ACD) cells, conjunctive cells *Adder*, conjunctive cells *Subtractor*, and position encoder. Each component of the calibration circuit is explained in further detail below, which contains its structure, functionality, and the firing behavior.

4.4.1. Visual detector

The visual detector is an abstract block governing the whole visual perception process of a visual cue in the environment. It solely represents the visual input signal that stimulates the ECD cells. This is based on the assumption that animals use extracted visual features of landmarks instead of the whole configuration of a landmark as the visual cue [29]. This assumption is also used by other calibration models described in Section 3.

4.4.2. Cue direction cells

This paper uses the same model to construct both the ECD cells and ACD cells, which represent the egocentric and allocentric angular direction of a visual landmark, respectively. Examples are visualized in Fig. 4. Each neuron's activity depends on the bearing of a visual landmark relative to the agent's orientation and position within the environment. Take the ECD cells module as an example, it contains n neurons and numbered with $i \in \{0, \dots, n-1\}$. α_i describes each neuron's preferred egocentric cue direction around the circle in the interval $[0, 2\pi)$ as

$$\alpha_i = \frac{2\pi i}{n}. \tag{3}$$

The angular distance $\Delta\alpha_{iL}$ between the cue (Landmark) and α_i in the egocentric frame is defined as

$$\Delta\alpha_{iL} = \alpha_L - \alpha_i, \tag{4}$$

where α_L is the egocentric direction of the cue. According to [43], its firing activity $f(\Delta\alpha_{iL})$ can be governed by

$$\begin{aligned} f(\Delta\alpha_{iL}) &= A + Be^{K\cos(\Delta\alpha_{iL})} \\ &= 1.72 + 0.344e^{5.29\cos(\Delta\alpha_{iL})}. \end{aligned} \tag{5}$$

A is the background firing rate and Be^K is the peak firing rate. K is a parameter to control the shape of the activity curve. The peak firing rate and the background firing rate are defined as 70 Hz and 1.72 Hz to mimic the data recorded from in-vivo neurons [44]. The highest firing rate arises at the neuron whose preferred cue direction is closest to the angular direction of the landmark. The lowest activity appears at the cue direction cell that is the furthest away from the landmark's position.

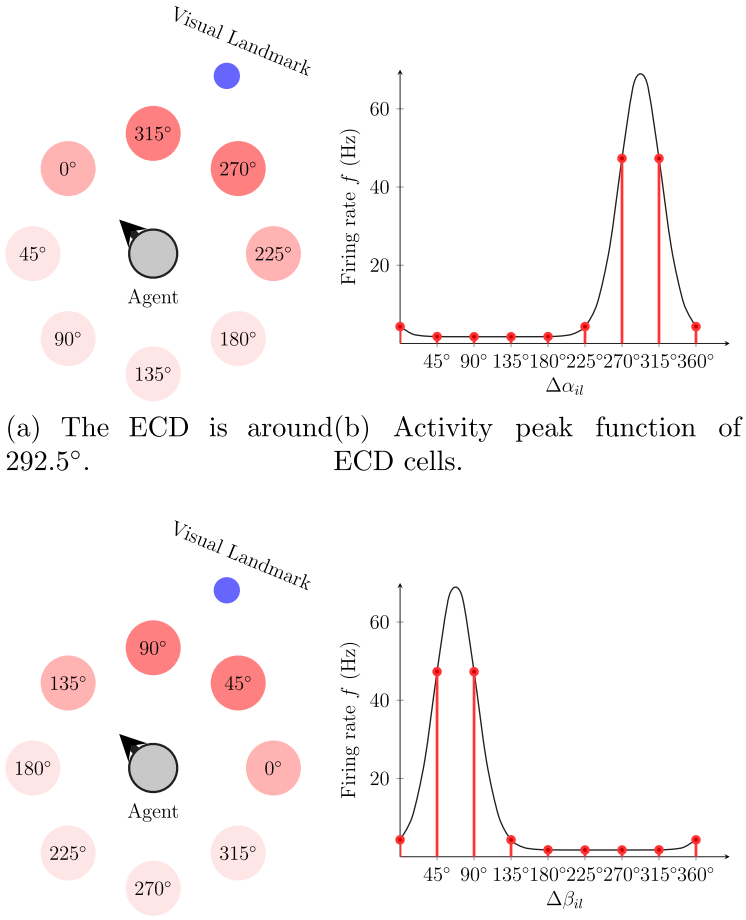

(a) The ECD is around 292.5°.

(b) Activity peak function of ECD cells.

(c) The ACD is around 67.5°.

(d) Activity peak function of ACD cells.

Fig. 4. ECD and ACD illustration for one example of spatial relation between the agent and the visual landmark.

The ACD cells share the same model and parameters as the ECD cells and its preferred allocentric cue direction is defined as β_i. Therefore, its activity $f(\Delta\beta_{iL})$ is calculated as

$$f(\Delta\beta_{iL}) = A + Be^{Kcos(\Delta\beta_{iL})} = 1.72 + 0.344e^{5.29cos(\Delta\beta_{iL})}, \quad (6)$$

where $\Delta\beta_{iL} = \beta_L - \beta_i$ and β_L is the allocentric direction of the cue. An example of the firing behavior of the ECD and ACD rings is illustrated in Figs. 4(b) and 4(d).

4.4.3. Conjunctive cell Adder

The task of the conjunctive cells in the calibration mechanism is to serve as a bridge between the egocentric and allocentric reference frame. In this case, the input information, ECD and HD, are used to compute the ACD of a landmark, which is subsequently encoded by the ACD cells. Therefore, this conjunctive cell field is also referred to as the *Adder*. Fig. 1 shows an example relation between an agent and a visual landmark. The agent's orientation is $\theta_A = 90°$. The landmark is perceived at $\alpha_L = 30°$ from the agent's pose. The ACD from the agent's position is $\beta_L = 120°$. The mathematical relation between these three variables is governed by

$$\beta_L = (\theta_A + \alpha_L) \mod 360° \quad (7)$$

As illustrated in Fig. 5a, the conjunctive cell *Adder* consists of n conjunctive cells aligned in a two-dimensional grid. The neurons are numbered with $i \in \{0, \dots, n-1\}$. Each row and each column consists of $\sqrt{n}$ neurons. Each neuron is associated with two inputs: the HD of the agent and the ECD of a visual landmark in the environment. The represented ECD α_i and HD θ_i of neuron i are governed by

$$\alpha_i = \frac{2\pi}{\sqrt{n}}(i \mod \sqrt{n}) \quad (8)$$

$$\theta_i = \frac{2\pi}{\sqrt{n}}(\sqrt{n} - 1 - (i \operatorname{div} \sqrt{n})), \quad (9)$$

where "mod" stands for the modulo operation and "div" stands for the integer division operation. The activity function for each neuron in the *Adder* is given by

$$f(\Delta\alpha_{iL}, \Delta\theta_{iA}) = A + Be^{0.5K(cos(\Delta\alpha_{iL})+cos(\Delta\theta_{iA}))} = 0.0504e^{2.645(cos(\Delta\alpha_{iL})+cos(\Delta\theta_{iA}))} \quad (10)$$

The lowest and the peak firing rate are set to 0 Hz and 10 Hz according to the measured values in [38]. This *Adder* describes a two-dimensional activity peak that emerges in the conjunctive cell field and combines information about HD and ECD at the same time. For example, an *Adder* with 36 neurons is visualized in Fig. 5a. The conjunctive cells show a two-dimensional activity peak with the peak firing rate at the intersection of the ECD $\alpha_L = 30°$ and HD $\theta_A = 90°$. The intensity of the neural activity is represented with the gradation of color red. Each ACD cell integrates the accumulated neuron firing rates via the diagonal input connections. The neuron number $i = 2$ of the ACD ring receives the largest input as it lies in the diagonal extension of the two-dimensional activity peak. Finally, an activity peak emerges in the ACD ring that encodes the ACD of the landmark. In this case, the resulting activity peak encodes $\beta_L = 120°$, which equals to the operation in (7).

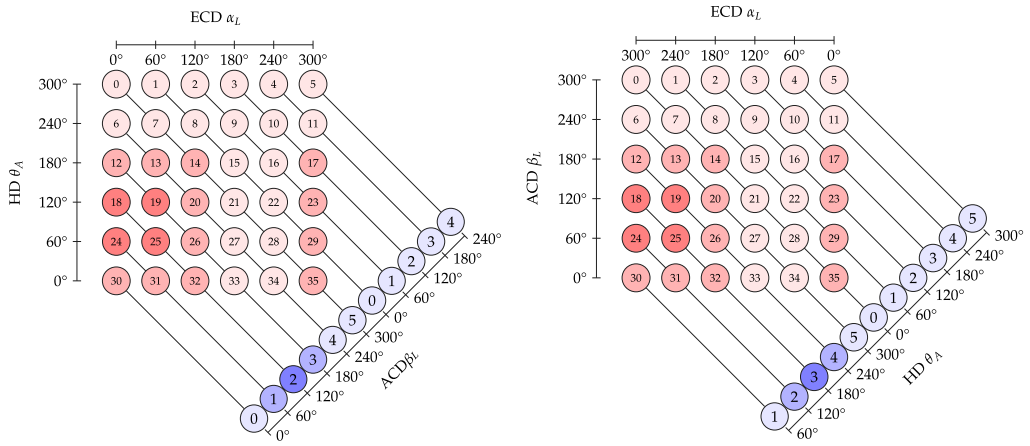

(a) Exemplary setup and activity of the *Adder*. (b) Example setup and activity of the *Subtractor*.

Fig. 5. Exemplary setup and activity of both conjunctive cells.

4.4.4. Conjunctive cell Subtractor

The conjunctive cell *Subtractor* also exhibits a similar two-dimensional activity profile as the *Adder*. In contrast, the purpose of the *Subtractor* is to perform a subtraction to obtain a feedback signal for resetting the HD signal. Therefore, the *Subtractor* takes ACD and ECD as the input to generate the HD signal according to

$$\theta_A = (\beta_L - \alpha_L + 360°) \mod 360° \tag{11}$$

Therefore, each conjunctive cell's activity corresponds to a certain ECD α_i and ACD β_i. The represented ECD and ACD of neuron i can be obtained by

$$\alpha_i = \frac{2\pi}{\sqrt{n}}(\sqrt{n} - 1 - (i \bmod \sqrt{n})) \tag{12}$$

$$\beta_i = \frac{2\pi}{\sqrt{n}}(\sqrt{n} - 1 - (i \operatorname{div} \sqrt{n})) \tag{13}$$

These angular distances determine the activity of neuron i according to

$$\begin{aligned} f(\Delta\alpha_{iL}, \Delta\beta_{iL}) &= A + Be^{0.5K(cos(\Delta\alpha_{iL})+cos(\Delta\beta_{iL}))} \\ &= 0.0504e^{2.645(cos(\Delta\alpha_{il})+cos(\Delta\beta_{il}))} \end{aligned} \tag{14}$$

For example, a *Subtractor* with 36 neurons is visualized in Fig. 5b, where the ECD direction is set to $\alpha_L = 270°$ and ACD to $\beta_L = 90°$. Thus, the HDC $i = 3$ receives the largest input as it lies on the diagonal extension of the two-dimensional activity peak of the conjunctive cells, and therefore is the most active HDC. In conclusion, this setup of neurons is capable of calculating the HD feedback signal with given ECD and ACD.

4.4.5. Position encoder

The position encoder stores the local allocentric position of the agent in relation to the position of the visual landmark, and additionally interacts with the ACD cells. First, it reads out the encoded ACD information from the ACD cells and associates it with the allocentric position of the agent. Second, it restores the ACD information according to the agent's position, and subsequently resets the firing activity in the ACD cells. However, it should be noted that the position encoder is not modeled in a biologically plausible way and its functionality is only abstractly defined.

4.5. Synaptic weight

The calculation of the synaptic weights between the components of the calibration circuit is adapted from [18], which aims to obtain a stable activity described by the firing rate model of each cell type (See (5), (6), (10), and (14)). The input current u_i at each post-synaptic neuron i is determined by summing up the input firing rates f_j from the pre-synaptic neurons j multiplied with their corresponding connection weights w_{ij}. Hence, the connection weights need to be adjusted so that the desired input current u_i is reached. In [18], the continuous error function describing the difference between the desired input currents and obtained input currents is defined in the Fourier domain as

$$E = \sum_{a=0}^{n-1} |\hat{u}_a - \hat{w}_a \hat{f}_a|^2 + \lambda \sum_{a=0}^{n-1} |\hat{w}_a|^2. \tag{15}$$

$\hat{u}_a$, $\hat{f}_a$, and $\hat{w}_a$ are the ath Fourier coefficient of the input current vector, firing rate vector, and the synaptic weight vector, respectively. λ is a regularization factor to control the shape of the weight function. The objective goal is to minimize the error E and the synaptic weight can be calculated in the Fourier domain by solving $\frac{dE}{d\hat{w}_a} = 0$. Therefore, the synaptic weight can be described as

$$\hat{w}_a = \frac{\hat{u}_a \hat{f}_a}{\lambda + |\hat{f}_a|^2}. \tag{16}$$

Detailed explanations can be found in [18,43]. According to (2), the desired input current u can be calculated as $\Phi^{-1}(f)$. Then, the pseudocode for calculating the synaptic weight is given in Algorithm 1. Since all the synaptic weights in the calibration circuit can be calculated by following this general procedure and the limited page space, we omit the detailed descriptions of the weight calculations and only provide the code of our algorithm at here.[1]

5. HDC calibration mechanism

The HDC calibration model consists of two mechanisms that work in parallel: the feedback loop and the ACD control.

5.1. Feedback loop

As shown in Fig. 3, the feedback loop consists of HDCs, ECD cells, the *Adder*, the *Subtractor*, and ACD cells. The feedback loop covers two functionalities. On the one hand, it calculates the ACD information with the ECD and HD information. On the other hand, it resets the activity of the HDCs according to the activity in the ECD cells and ACD cells. The feedback loop is driven by two inputs. The first input is the angular velocity that will be integrated by the HDCs. The second input is the

[1] https://github.com/BZSROCKETS/HDC_calibration.

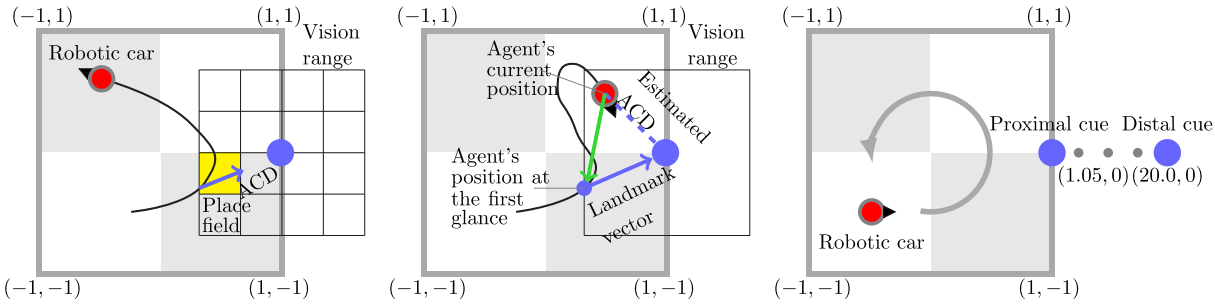

(a) Simple place encoding feedback. (b) Place encoding with first glance learning. (c) Toy environment.

Fig. 6. (a) The agent associated one ACD to the yellow colored place field when the agent perceived the visual landmark the first time in this place field. When revisiting this yellow place field, the associated ACD is used to restore the ACD cells' activity. (b) The position encoder stored the agent's position from the first glance and the landmark vector which is created with distance and ACD information. The ACD in the agent's current position is estimated by adding the vector to the agent's position from the first glance (green) to the landmark vector. (c) Visualization of the toy environment. Either a proximal visual cue or a distal visual cue is used in this environment.

Algorithm 1: Calculate Connection Weights

Input: n: number of neurons
λ: flatness parameter
Λ: vector containing flatness parameters λ
F: desired firing rates of n presynaptic neurons
U: desired currents of n post-synaptic neurons
E: summation of squared error for λ
Output: W_{opt}: the optimal connection weights
initialize E with infinity
$E := \infty$;
compute Fourier transforms (FFT)
$\hat{F} := \text{FFT}(F)$;
$\hat{U} := \text{FFT}(U)$;
for λ *in* Λ **do**
  # calculate the Fourier coefficients of W
  for $i = 0...n-1$ **do**
    $\hat{W}[i] = \frac{\hat{U}[i]\hat{F}[i]}{\lambda + |\hat{F}[i]|^2}$;
  end
  # compute the inverse Fourier transformation
  $W := \text{FFT}(\hat{W})$;
  # compute the sum of squared errors and store it
  $X := \sum_{i=0}^{n-1}(U[i] - W[i]F[i])^2 + \frac{1}{\lambda}$;
  if $E > X$ **then**
    $W_{opt} := W$;
    $E = X$;
  end
end
return W_{opt};

visual information when a visual landmark is in the agent's field and range of vision. Depending on the presence of a visual landmark, the feedback loop will be switched on or off.

If both inputs are present, the HD ring and the ECD ring project onto the *Adder*, which in turn stimulates the ACD ring. Then, the ACD cells and the ECD cells project together onto the *Subtractor*, which computes the HD feedback signal. This means that the HDCs receive input that is based on the activity in the ACD cells and ECD cells. If there is no landmark visible to the agent, the visual detector will not project on the ECD cells and no activity peak will emerge at the ECD cells. Therefore, no feedback signal will be created, as the *Subtractor* is driven by the ACD cells and the ECD cells that exhibit no activity peak.

5.2. Allocentric cue direction control

When the feedback loop is switched on, the position encoder will interact with the ACD cells. It can either store ACD information or reset the activity in the ACD cells according to previously restored ACD information. The processing of reading and resetting the ACD information can be conducted using two alternative strategies, namely the place-encoding feedback based on place field matrix (PFM-based calibration) [20] and our proposed place encoding feedback based on the first glance learning (FGL-based calibration). In both modes, the position encoder stores the ACD information, which is obtained by egocentrically observing a visual landmark. Subsequently, the stored ACD information is used to correct the accumulative HD errors when observing the visual landmark again.

PFM-based calibration. The idea of PFM-based calibration was developed in [20] and is adapted as a benchmark for comparison in this paper. The allocentric direction of the cue (ACD) is encoded via a place field matrix, in which each matrix element corresponds to a certain squared spatial area around the landmark, as illustrated in Fig. 6(a). The center of the place field matrix is placed at the position of the visual cue and the space covered by the matrix is decided by the visual field of the agent. The number of place fields can be finely tuned. In the example in Fig. 6(a), the dimension of one place field is set to 1 unit and the matrix covers 4 × 4 units. Each place field will store the ACD information when the agent is in this field and it will reset the activity ACD cells with the encoded ACD information, when the agent revisits this place field again. However, the error of this method is highly related to the fineness of the place field matrix.

FGL-based calibration. We propose the first glance learning (FGL) mechanism, in which the position encoder stores all the necessary information of a visual landmark at once, which is visualized in Fig. 6(b). When a landmark is perceived by the agent for the first time, the position encoder stores the distance vector between the agent and the visual cue as well as the ACD information. The agent will reset its HD once the cue is observed again within its visual field at any place. To reset the HD, the agent performs a distance vector addition to estimate the current ACD at the new location where it perceives the cue again. Subsequently, this newly obtained ACD is used to reset the ACD cells' activity, which is used to reset the HD via the *Subtractor*.

The idea of this mechanism is to allow the agent to calibrate the HD error as soon as a visual cue is perceived, while only storing information that animals can infer using their senses. As supported by neurobiology findings, the distance vector between the agent and the landmark can be obtained with grid cells and visual perception. However, in

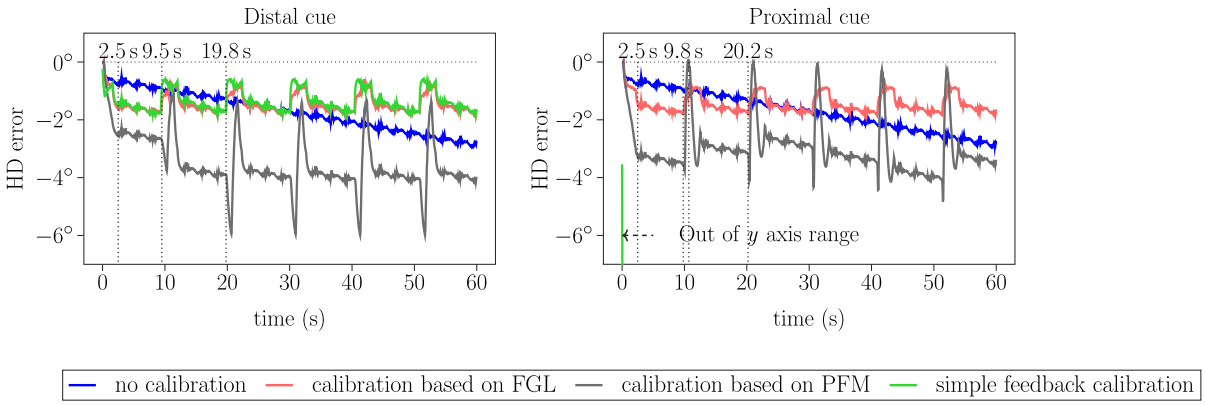

Fig. 7. HD error plot for a 60 s run in the toy environment. Left: A distal cue is placed at position $(20, 0)$. The timestamps 9.5 s and 19.8 s indicate exemplary moments when the visual landmark is in sight. The timestamp 2.5 s describes the last moment when the visual landmark is in sight during the first circular turn of the agent. Right: A proximal cue is placed at $(1.05, 0)$. The timestamps 9.8 s and 20.2 s indicate example moments when the visual landmark falls in sight. Timestamp 2.5 s describes the last moment when the visual landmark falls in sight in the first circular turn of the agent.

this work, this distance vector information is directly acquired from simulation or real-world experiments, which is out of our scope. Thus, this mode accounts more for mimicking the calibration behavior found from animals than designing a neural vector computing circuit.

6. Experiments

In this section, we will evaluate the performance of the proposed HDC calibration network in both simulations and real-world implementations.

6.1. Simulations

All the simulation tasks are performed in PyBullet [45], in which a simulated mobile robot is controlled to move in an environment with one visual landmark. The robot is equipped with 16 proximity sensors that are circularly distributed around itself and used to detect any obstacles. Then, with the help of a Braitenberg controller [46], the robot is able to move freely without colliding with any walls. One camera with a viewing angle of 90° is mounted on the top of the robot to perceive visual landmarks. The HDC calibration network is simulated with a step size of 0.5 ms. The PyBullet is simulated with a step size of 50 ms. In each task, four approaches are tested, namely, no HDC calibration, simple feedback calibration, place-encoding calibration based PFM, and the proposed place encoding calibration based on first glance learning.

The toy simulation environment is a square box with the upper left corner positioned at $(-1, 1)$ and the lower right corner at $(1, -1)$ (See Fig. 6(c)). The blue circle placed in the environment represents the visual landmark. The agent is initially placed at $(0, -0.5)$ and oriented to the right (normal vector $(1, 0)$ which corresponds to 0°). Each episode is set to 60 s, during which the agent is able to drive almost six full counterclockwise circles. The agent's angular velocity varies between $20°/s$ and $40°/s$ over time.

6.1.1. Distal landmark

In the first simulation environment, the box contains a distal visual landmark at $(20, 0)$. The resulting HD errors over time are plotted in Fig. 7. All four calibration setups show negative HD errors, which indicates that the shift of the HDCs' activity peak falls behind of the steering of the agent due to its own neural dynamics. The blue curve shows the HD error evolving over time with no calibration. The HD error increases limitlessly with a slope of $-0.05°/s$. In contrast, all the other three calibration methods limit the HD error to a lower bound.

The FGL-based calibration and the simple feedback calibration show the best accuracy in an environment with a distal landmark. While, the PFM-based calibration performs the least accurately and exhibits HD errors up to −6°. Since the robot starts at a position where the visual landmark is in sight, the feedback loop is active from the beginning of each episode. The landmark is in sight until 2.5 s in the first lap. During this period, the feedback loop will introduce additional errors than the setting with no calibration, since its internal computation is based on the HD and ECD information that are already a few steps old. In this phase, the ACD information is associated with the visited place fields. Therefore, the smallest error included in the ACD is generated right at the beginning of the episode, which is around −1°. When the landmark is out of sight (e.g., from 2.5 s to 9.5 s), the HD errors of all three calibration models increase over time with the same slope as the model without calibration. When the agent perceives the landmark again (at 9.5 s, 19.8 s, etc.), the simple feedback calibration immediately calibrate the HD error to −0.8°, which resets the HD via direct projections from the ECD cells, whenever the landmark is in the agent's vision field. As the landmark is not in infinite distance, small parallax errors are introduced for the simple feedback calibration. At the same time, the FGL-based calibration also starts to calibrate and maintain at a level with very small errors until the visual cue is out of sight. For the PFM-based calibration, the HD error increases first and right after this, the ACD corresponding to the currently occupied place field is restored and used to reset the HD signal to almost −1°. During the calibration phase (e.g. from 9.5 s until ≈13 s), the HD error increases again due to the limitation of the PFM method. The calibration accuracy is highly related to the granularity of the place field matrix, in which one unit vector describes the ACD information that is associated with this place field. However, the agent may be located at different positions within one single place field. Hence, the associated unit vector to a place field cannot accurately represent the ACD at different positions within one place field. Therefore, parallax errors are introduced when the agent revisits a known place field but traverses positions that are different from the first time when the ACD is stored.

6.1.2. Proximal landmark

In the second setup, a proximal visual landmark is placed at position $(1.05, 0)$. The experiment results are also shown in Fig. 7. The FGL-based calibration performs on the same level as the task when using the distal landmark, which demonstrates its applicability to either proximal or distal visual cues. As explained above, the simple feedback calibration is not applicable to tasks with proximal cues, as it introduces an error over −25°, which is not fully visualized in Fig. 7. The place encoding calibration performs slightly better than with the distal landmark, but still introduces a larger error than the path integration.

Based on the evaluation results in the toy environment, we can conclude that the simple feedback calibration mechanism is not applicable in environments with proximal cues. The PFM-based calibration

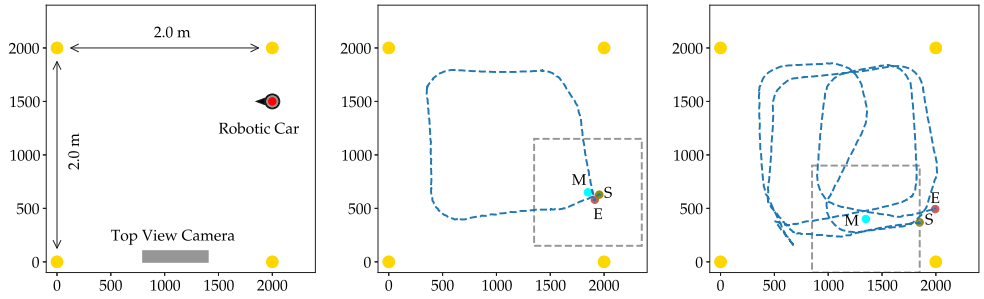

(a) Illustration of the real-world setup. (b) Run 1: agent's trajectory and landmark position. (c) Run 2: agent's trajectory and landmark position.

Fig. 8. Illustration of the real-world experiment setup and the trajectories of the robot. The dark blue graph shows the route of the agent. Marker "M", "S", and "E" represent the position of the landmark, starting position, and the ending position, respectively. The gray dashed square shows the visible field of the landmark. The four yellow stickers are used as referential points to infer the agent's position (red sticker) during a run.

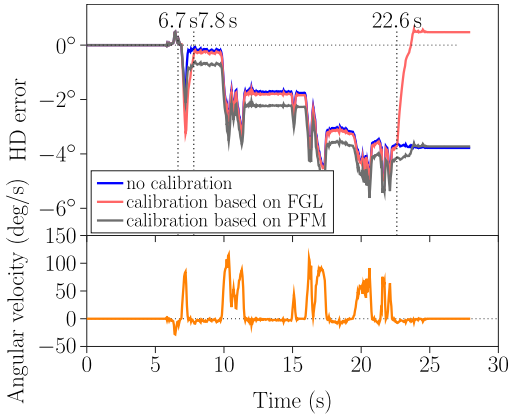

(a) Run 1: The interval between the timestamps 6.7 s and 7.8 s indicate a phase when the landmark is in sight of the agent. Timestamp 22.6 s indicates the moment that the landmark is in sight again when the agent returns to the end.

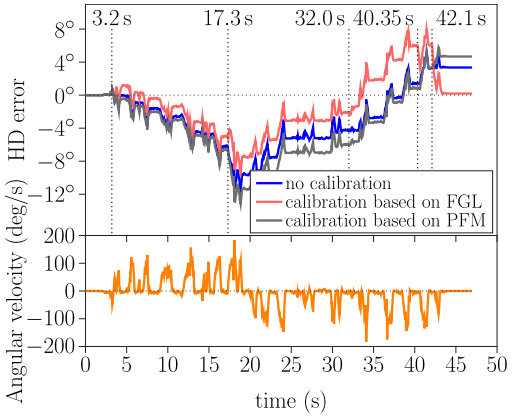

(b) Run 2: The timestamps indicate the moments when the visual landmark starts to be in sight of the agent.

Fig. 9. Illustration of the HD error and the corresponding angular velocity during each run in the real-world experiment.

is able to calibrate the HD error with a limited bound, but does not perform well compared with the proposed mechanism based on FGL, which can calibrate the HD error with high accuracy (less than 2°). Note the measurement noise is fully considered and the performance of the proposed method is proved to be robust against the noise. In the following section, we will further show the performance of the proposed method with real-world noise generated from IMU sensors.

6.2. Real-world experiments

The proposed HDC calibration model is also evaluated in the real world by performing an indoor robotic navigation task, which is illustrated in Fig. 8. The robotic car is equipped with a Raspberry Pi that receives drive commands from the human operator. The on-board inertial measurement unit (IMU, BNO055 [47]) is used to track the ground truth of the directional heading and the angular velocity of the robot. The angular velocity is used to estimate the directional heading of the robot by using the HDC model proposed in [43]. An RGB camera mounted above the experiment field is used to track the position of the car, in relation to the coordination system that is set up by four yellow markers on the floor. A proximal visual landmark is placed in the middle of the field and it can only be observed within a minimum range of 0.5 m, which means the visual landmark is approximately visible to the agent only when the agent is located within the dashed square in Fig. 8. The positions of the landmark are set separately for each run to ensure that the agent perceives the landmark from different angles in different runs. The number of the place field matrix elements that are used for the PFM-based calibration is set to 3000 × 3000.

6.2.1. First run

In the first run, the agent is manually controlled to run along one single circle. The trajectory of the robot is shown in the middle of Fig. 8(b). The landmark is positioned at (1850, 650), which is represented by the marker "M". The starting position and end position are marked by "S" and "E", respectively. Therefore, the agent is able to perceive the visual landmark twice in this single lap. The angular velocity during this run is shown in Fig. 9(a), which is up to 120 °/s. Fig. 9(a) also shows the HD errors of three different calibration methods, namely, no calibration (path integration), PFM-based calibration, and FGL-based calibration. The simple feedback calibration is not evaluated in the real world, since it is not applicable to tasks with proximal cues. The agent starts to turn at 6 s and perceives the visual landmark for the first time from 6.7 s to 7.8 s. When the robot discovers the visual landmark for the first time, the calibration mechanism introduces an HD error due to the information delay in the feedback loop of the proposed system. The FGL-based place encoding calibration model

quickly reduces the HD error to reach almost the same error level as the model without calibration at 7.8 s. In contrast, the PFM-based calibration keeps a constant offset to the blue line describing the HD error of the model without calibration, since it is only able to calibrate the HD error in a new view of the landmark at the same place field. The landmark is out of sight after 7.8 s and perceived for the second time at 22.6 s. Then, the FGL-based calibration model resets the HD error to 0.48°. The reason for the small error at the end arises from the parallax error introduced while one-shot learning the landmark vector at the beginning of the episode. However, it limits the HD error to a maximum, and therefore, improves the performance compared to the model with no calibration and to the PFM-based calibration. The blue and the gray graph show almost the same HD error at the end. As the agent does not revisit the same place field when the agent has another view on the landmark, the PFM-based calibration never restores the ACD to calibrate. It can be concluded that the calibration model using FGL performs best as it resets the HD error when the landmark is seen for a second time.

6.2.2. Second run

The second run is performed to evaluate calibration models when an agent revisits a landmark several times, and additionally performs one phase of left turns as well as one phase of right turns. Fig. 8(c) shows the trajectory of the agent and its starting position and end position. The landmark is placed at (1350, 400). The HD error and the angular velocity are plotted in Fig. 9(b). The agent starts to turn left until 20 s and continues to turn right with a negative angular velocity. At 3.2 s the agent perceives the landmark for the first time. In this phase, both calibration models activate the feedback loop, and therefore introduce a parallax error in the HD signal. From this moment, the offset between all curves stays almost constant through the path integration phase until 40.35 s. The PFM-based calibration increases the HD error as the agent perceives the visual landmark in a new place field. In contrast, the FGL-based calibration is able to reduce the HD error at this point. In line with the results from the first run, the calibration model using FGL achieves the lowest HD error at the end. However, the model without calibration performs second best, and thus better than the PFM-based calibration. The reason is that the agent is not revisiting a place field in which it already had a look at the visual landmark.

7. Conclusion

This paper presents a biologically plausible HD calibration model, which uses visual landmarks to calibrate the HD error introduced by path integration. Our HD calibration model can transform the directional information of a visual cue from the egocentric coordination system to the allocentric coordination system, with the help of the HD information of the agent in the allocentric coordination system. Therefore, by associating the position information of the agent with the allocentric direction information of a visual cue, our method allows the agent to calibrate its internal sense of the direction when revising a known visual landmark. The experimental results demonstrated great performance in terms of accuracy for calibrating the directional heading and real-world capability compared with previous studies.

Declaration of competing interest

The authors declare that they have no known competing financial interests or personal relationships that could have appeared to influence the work reported in this paper.

Data availability

No data was used for the research described in the article.

Acknowledgments

This project/research has received funding from the European Union's Horizon 2020 Framework Programme for Research and Innovation under the Specific Grant Agreement No. 945539 (Human Brain Project SGA3) also funded by Pazhou Lab PZL2021KF0020.

References

[1] S. Poulter, T. Hartley, C. Lever, The neurobiology of mammalian navigation, Curr. Biol. 28 (17) (2018) R1023–R1042.
[2] L.L. Rogers, Homing Tendencies of Large Mammals: a Review, Wisconsin Humane Society, Translocation of Wild Animals. Milwaukee, 1988, pp. 76–92.
[3] L.I. Avens, Homing Behavior, Navigation, and Orientation of Juvenile Sea Turtles, The University of North Carolina at Chapel Hill, 2003.
[4] H.G. Wallraff, Navigation by homing pigeons: updated perspective, Ethol. Ecol. Evol. 13 (1) (2001) 1–48.
[5] R.E. Henshaw, R.O. Stephenson, Homing in the gray wolf (Canis lupus), J. Mammal. 55 (1) (1974) 234–237.
[6] S.J. Julier, J.K. Uhlmann, Building a million beacon map, in: Sensor Fusion and Decentralized Control in Robotic Systems IV, Vol. 4571, International Society for Optics and Photonics, 2001, pp. 10–21.
[7] J. Ranck Jr., Head direction cells in the deep layer of dorsal presubiculum in freely moving rats, in: Society of Neuroscience Abstract, Vol. 10, 1984, p. 599.
[8] D. Derdikman, J.R. Whitlock, A. Tsao, M. Fyhn, T. Hafting, M.-B. Moser, E.I. Moser, Fragmentation of grid cell maps in a multicompartment environment, Nature Neurosci. 12 (10) (2009) 1325–1332.
[9] K. Diba, G. Buzsáki, Forward and reverse hippocampal place-cell sequences during ripples, Nature Neurosci. 10 (10) (2007) 1241–1242.
[10] S. Riisgaard, M.R. Blas, SLAM for dummies, Tutor. Approach Simul. Localiz. Map. 22 (1–127) (2003) 126.
[11] J.S. Taube, R.U. Muller, J.B. Ranck, Head-direction cells recorded from the postsubiculum in freely moving rats. I. Description and quantitative analysis, J. Neurosci. 10 (2) (1990) 420–435.
[12] R.M. Yoder, J.S. Taube, Head direction cell activity in mice: robust directional signal depends on intact otolith organs, J. Neurosci. 29 (4) (2009) 1061–1076.
[13] G.M. Muir, J.E. Brown, J.P. Carey, T.P. Hirvonen, C.C. Della Santina, L.B. Minor, J.S. Taube, Disruption of the head direction cell signal after occlusion of the semicircular canals in the freely moving chinchilla, J. Neurosci. 29 (46) (2009) 14521–14533.
[14] J.S. Taube, The head direction signal: origins and sensory-motor integration, Annu. Rev. Neurosci. 30 (2007) 181–207.
[15] R.G. Robertson, E.T. Rolls, P. Georges-François, S. Panzeri, Head direction cells in the primate pre-subiculum, Hippocampus 9 (3) (1999) 206–219.
[16] S. Valerio, J.S. Taube, Path integration: how the head direction signal maintains and corrects spatial orientation, Nature Neurosci. 15 (10) (2012) 1445–1453.
[17] J.P. Goodridge, P.A. Dudchenko, K.A. Worboys, E.J. Golob, J.S. Taube, Cue control and head direction cells., Behav. Neurosci. 112 (4) (1998) 749.
[18] K. Zhang, Representation of spatial orientation by the intrinsic dynamics of the head-direction cell ensemble: a theory, J. Neurosci. 16 (6) (1996) 2112–2126.
[19] W. Skaggs, J. Knierim, H. Kudrimoti, B. McNaughton, A model of the neural basis of the rat's sense of direction, Adv. Neural Inf. Process. Syst. (ISSN: 1049-5258) 7 (1995) 173–180.
[20] A. Bicanski, N. Burgess, Environmental anchoring of head direction in a computational model of retrosplenial cortex, J. Neurosci. 36 (46) (2016) 11601–11618.
[21] A. Arleo, W. Gerstner, Modeling rodent head-direction cells and place cells for spatial learning in bio-mimetic robotics, From Anim. Anim. 6 (2000) 236–245.
[22] M.J. Milford, G.F. Wyeth, D. Prasser, RatSLAM: a hippocampal model for simultaneous localization and mapping, in: IEEE International Conference on Robotics and Automation, 2004. Proceedings. ICRA'04. 2004, Vol. 1, IEEE, 2004, pp. 403–408.
[23] Y. Lozano Navarro, Landmark Processing by Head Direction Cells (Ph.D. thesis), UCL (University College London), 2016.
[24] A.D. Redish, et al., Beyond the Cognitive Map: From Place Cells to Episodic Memory, MIT Press, 1999.
[25] D. Jain, I.R. Jakhalekar, S.S. Deshmukh, Navigational strategies and their neural correlates, J. Indian Inst. Sci. 97 (4) (2017) 511–525.
[26] C.R. Gallistel, The Organization of Learning, The MIT Press, 1990.
[27] B.L. McNaughton, F.P. Battaglia, O. Jensen, E.I. Moser, M.-B. Moser, Path integration and the neural basis of the 'cognitive map', Nat. Rev. Neurosci. 7 (8) (2006) 663–678.
[28] R.M. Yoder, B.J. Clark, J.E. Brown, M.V. Lamia, S. Valerio, M.E. Shinder, J.S. Taube, Both visual and idiothetic cues contribute to head direction cell stability during navigation along complex routes, J. Neurophysiol. 105 (6) (2011) 2989–3001.
[29] J.J. Knierim, D.A. Hamilton, Framing spatial cognition: neural representations of proximal and distal frames of reference and their roles in navigation, Physiol. Rev. 91 (4) (2011) 1245–1279.

[30] T. Wolbers, J.M. Wiener, Challenges for identifying the neural mechanisms that support spatial navigation: the impact of spatial scale, Front. Hum. Neurosci. 8 (2014) 571.
[31] A. Arleo, L. Rondi-Reig, Multimodal sensory integration and concurrent navigation strategies for spatial cognition in real and artificial organisms, J. Integr. Neurosci. 6 (03) (2007) 327–366.
[32] Z. Bing, C. Meschede, F. Röhrbein, K. Huang, A.C. Knoll, A survey of robotics control based on learning-inspired spiking neural networks, Front. Neurorobot. 12 (2018) 35.
[33] Z. Bing, C. Meschede, G. Chen, A. Knoll, K. Huang, Indirect and direct training of spiking neural networks for end-to-end control of a lane-keeping vehicle, Neural Netw. 121 (2020) 21–36.
[34] P.-Y. Jacob, G. Casali, L. Spieser, H. Page, D. Overington, K. Jeffery, An independent, landmark-dominated head-direction signal in dysgranular retrosplenial cortex, Nature Neurosci. 20 (2) (2017) 173–175.
[35] H.J. Page, D.M. Walters, R. Knight, C.E. Piette, K.J. Jeffery, S.M. Stringer, A theoretical account of cue averaging in the rodent head direction system, Philos. Trans. R. Soc. B 369 (1635) (2014) 20130283.
[36] A. Bicanski, N. Burgess, A neural-level model of spatial memory and imagery, eLife 7 (2018) e33752.
[37] P. Byrne, S. Becker, N. Burgess, Remembering the past and imagining the future: a neural model of spatial memory and imagery, Psychol. Rev. 114 (2) (2007) 340.
[38] A.A. Wilber, B.J. Clark, T.C. Forster, M. Tatsuno, B.L. McNaughton, Interaction of egocentric and world-centered reference frames in the rat posterior parietal cortex, J. Neurosci. 34 (16) (2014) 5431–5446.
[39] C. Wang, X. Chen, H. Lee, S.S. Deshmukh, D. Yoganarasimha, F. Savelli, J.J. Knierim, Egocentric coding of external items in the lateral entorhinal cortex, Science 362 (6417) (2018) 945–949.
[40] B.L. McNaughton, J.J. Knierim, M.A. Wilson, Vector encoding and the vestibular foundations of spatial cognition: neurophysiological and computational mechanisms, 1995.
[41] J. O'Keefe, J. Dostrovsky, The hippocampus as a spatial map: preliminary evidence from unit activity in the freely-moving rat, Brain Res. (1971).
[42] T. Zeng, F. Tang, D. Ji, B. Si, NeuroBayesSLAM: Neurobiologically inspired Bayesian integration of multisensory information for robot navigation, Neural Netw. 126 (2020) 21–35.
[43] Z. Bing, A.E. Sewisy, G. Zhuang, F. Walter, F.O. Morin, K. Huang, A. Knoll, Towards cognitive navigation: Design and implementation of a biologically inspired head direction cell network, IEEE Trans. Neural Netw. Learn. Syst. (2021) http://dx.doi.org/10.1109/TNNLS.2021.3128380.
[44] U. Pereira, N. Brunel, Attractor dynamics in networks with learning rules inferred from in vivo data, Neuron 99 (1) (2018) 227–238.
[45] E. Coumans, Y. Bai, 2019. PyBullet, a python module for physics simulation for games, robotics and machine learning, 2016.
[46] Z. Bing, C. Meschede, K. Huang, G. Chen, F. Rohrbein, M. Akl, A. Knoll, End to end learning of spiking neural network based on r-stdp for a lane keeping vehicle, in: 2018 IEEE International Conference on Robotics and Automation, ICRA, IEEE, 2018, pp. 4725–4732.
[47] B. Sensortec, Intelligent 9-axis absolute orientation sensor, 2020, Rev. 17.

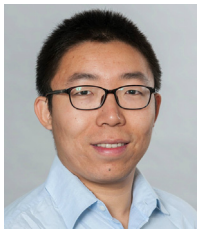

Zhenshan Bing received his doctorate degree in Computer Science from the Technical University of Munich, Germany, in 2019. He received his B.S degree in Mechanical Design Manufacturing and Automation from Harbin Institute of Technology, China, in 2013, and his M.Eng degree in Mechanical Engineering in 2015, at the same university.

Dr. Bing is currently a postdoctroal researcher with Informatics 6, Technical University of Munich, Munich, Germany. He also serves as an associated editor for IEEE Transactions on Neural Networks and Learning Systems. His research investigates the snake-like robot which is controlled by artificial neural networks and its related applications.

Dominik Nitschke is currently studying Computer Science at the Technical University of Munich as a master student. His research interest is artificial intelligence on robotics implementations, especially with biologically inspired learning algorithms.

Genghang Zhuang received his M.Eng degree in Software Engineering at Sun Yat-sen University, China, in 2019, and his B.Eng degree in Software Engineering at the same university in 2017. He is currently a doctoral student at Chair of Robotics, Artificial Intelligence and Real-time Systems, Department of Informatics, Technical University of Munich, Germany. His research interests include perception and planning in autonomous driving, especially with LiDAR sensors and biologically inspired methods.

Kai Huang joined Sun Yat-Sen University as a Professor in 2015. He was appointed as the director of the Institute of Unmanned Systems of School of Data and Computer Science in 2016. He was a senior researcher in the Computer Science Department, the Technical University of Munich, Germany from 2012 to 2015 and a research group leader at fortiss GmbH in Munich, Germany, in 2011. He earned his Ph.D. degree at ETH Zurich, Switzerland, in 2010, his MSc from University of Leiden, the Netherlands, in 2005, and his BSc from Fudan University, China, in 1999. His research interests include techniques for the analysis, design, and optimization of embedded systems, particularly in the automotive and robotic domains. He was awarded the Program of Chinese Global Youth Experts 2014 and was granted the Chinese Government Award for Outstanding Self-Financed Students Abroad 2010. He was the recipient of Best Paper Awards ESTC 2017, ESTIMedia 2013, SAMOS 2009, Best Paper Candidate ROBIO 2017, ESTMedia 2009, and General Chairs' Recognition Award for Interactive Papers in CDC 2009. He has served as a member of the technical committee on Cybernetics for Cyber-Physical Systems of IEEE SMC Society since 2015.

Alois Knoll (Fellow) received his diploma (M.Sc.) degree in Electrical/Communications Engineering from the University of Stuttgart, Germany, in 1985 and his Ph.D. (*summa cum laude*) in Computer Science from Technical University of Berlin, Germany, in 1988. He served on the faculty of the Computer Science department at TU Berlin until 1993. He joined the University of Bielefeld, Germany as a full professor and served as the director of the Technical Informatics research group until 2001. Since 2001, he has been a professor at the Department of Informatics, Technical University of Munich (TUM), Germany. He was also on the board of directors of the Central Institute of Medical Technology at TUM (IMETUM). From 2004 to 2006, he was Executive Director of the Institute of Computer Science at TUM. Between 2007 and 2009, he was a member of the EU's highest advisory board on information technology, ISTAG, the Information Society Technology Advisory Group, and a member of its subgroup on Future and Emerging Technologies (FET). His research interests include cognitive, medical and sensor-based robotics, multi-agent systems, data fusion, adaptive systems, multimedia information retrieval, model-driven development of embedded systems with applications to automotive software and electric transportation, as well as simulation systems for robotics and traffic.